Journal of Systems Engineering and Electronics
Vol. 35, No. 2, April 2024, pp.495 – 508

Fast solution to the free return orbit's reachable domain of the manned lunar mission by deep neural network

YANG Luyi[1,2], LI Haiyang[1,3], ZHANG Jin[1,3,*], and ZHU Yuehe[1,3]

1. College of Aerospace Science and Engineering, National University of Defense Technology, Changsha 410073, China;
2. China Astronauts Research and Training Center, Beijing 100094, China;
3. Hunan Key Laboratory of Intelligent Planning and Simulation for Aerospace Missions, Changsha 410073, China

Abstract: It is important to calculate the reachable domain (RD) of the manned lunar mission to evaluate whether a lunar landing site could be reached by the spacecraft. In this paper, the RD of free return orbits is quickly evaluated and calculated via the classification and regression neural networks. An efficient database-generation method is developed for obtaining eight types of free return orbits and then the RD is defined by the orbit's inclination and right ascension of ascending node (RAAN) at the perilune. A classify neural network and a regression network are trained respectively. The former is built for classifying the type of the RD, and the latter is built for calculating the inclination and RAAN of the RD. The simulation results show that two neural networks are well trained. The classification model has an accuracy of more than 99% and the mean square error of the regression model is less than 0.01° on the test set. Moreover, a serial strategy is proposed to combine the two surrogate models and a recognition tool is built to evaluate whether a lunar site could be reached. The proposed deep learning method shows the superiority in computation efficiency compared with the traditional double two-body model.

Keywords: manned lunar mission, free return orbit, reachable domain (RD), deep neural network, computation efficiency.

DOI: 10.23919/JSEE.2023.000117

1. Introduction

Lunar exploration and related scientific research have been heating up in recent years. The United States has proposed the Artemis program which aims to land the human on the Moon in 2024 and prepares for the next giant leap, the exploration of Mars[1,2]. In December 2020, China successfully implemented the lunar exploration mission of Chang'e-5, indicating that China mastered the lunar surface sampling and return technology [3]. It lays a solid foundation for China's manned lunar exploration mission in the future.

The manned lunar exploration mission is a complex engineering project and one of the key techniques is the design of lunar transfer orbits. The spacecraft in the cislunar space is mainly affected by the central gravity of multiple celestial bodies, non-spherical perturbative forces and solar pressure, resulting in the complex mechanical environment [4]. Zheng et al. [5] introduced the mission constraint and the flight mode of the manned lunar project. Peng et al. [6] presented six manned lunar landing flight modes by employing the space station. Topputo [7] proposed a direct transcription and multiple shooting strategy to solve the coplanar two-impulse Earth-Moon transfers in the restricted four-body model, and systematically concluded the variation of the velocity increment with the flight time. Lyu et al. [8] researched the two-impulse Earth-Moon transfers in the circular restricted three-body problem (CRTBP) based on a differential correction approach. Gao et al. [9] designed the two-impulse Earth-Moon trajectory by employing the lunar orbit station and analyzed orbital transfer windows in typical years. A special type of two-impulse Earth-Moon transfers is named the circumlunar free return orbit (FRO), which is quasi-symmetric about the Earth-Moon line in the cislunar space [10]. The FROs are usually employed by the manned spacecraft in order to guarantee the high safety of astronauts. Zhou et al. [11] studied the high-precision solution of the fixed-thrust FRO centered on rendezvous and docking with a lunar space station. Luo et al. [12] designed the FRO by an improved differential correction method.

On the basis of the Earth-Moon orbit design method, the reachable domain (RD) of orbits is important for the manned lunar mission implementation that could help select the lunar land site. For the spacecraft in low Earth orbit (LEO), the RD designates the collection of all positions accessible of the spacecraft under a given initial orbit and fuel constraint [13]. As for the RD in the

Manuscript received September 16, 2021.
*Corresponding author.
This work was supported by the National Natural Science Foundation of China (12072365) and the Natural Science Foundation of Hunan Province of China (2020JJ4657).

manned lunar mission, it is usually characterized as the reachable region of the lunar surface that could be reached by the lunar probe with mission constraints satisfied. Furtherly, the RD of the manned lunar mission can be defined as the high-dimensional domain of the characteristic orbital parameters of the lunar probe, such as the orbital inclination and right ascension of ascending node (RAAN) of the arrived lunar orbit [14,15]. Peng et al. [14] studied the parameter characteristics of the hybrid lunar transfer orbit and discussed the extension of the RD of the lunar surface. Li et al. [16] proposed the multi-segment FRO that was composed of the two-segment FROs and it could extend the RD of the lunar surface compared with the one-segment FRO. He et al. [17] studied the solution set of the Sun-perturbed optimal two-impulse trans-lunar orbit. Li et al. [18] investigated the site selection of manned lunar exploration and found that the RD influenced the strategy of the site selection considering engineering constraints. However, as for the computation of the RD in the manned lunar mission, the existing researches [14−17] mainly adopted the traversal shooting method with low efficiency. Moreover, the inherent mechanism and characteristics of the lunar RD have not been uncovered.

The practical engineering constraints in the manned lunar mission are strongly nonlinear, and the coupling mechanism between the lunar transfers and the RD is complex. Besides, it is difficult to achieve a balance between the solution accuracy and the computation efficiency for large-scale analysis. The artificial intelligence has developed rapidly, and especially the machine learning (ML) method has been successfully applied to regression (RG) statistics, classification (CL), prediction, cluster analysis, and so on. ML has been used in the field of astrodynamics such as fuel cost estimation, orbit CL, and orbit propagation [19]. Izzo et al. [20] used unsupervised ML methods to solve the multiple asteroid rendezvous problem and explained the nonlinear characteristics of the selection of the target asteroids. Uriot et al. [21] presented the design and results of the spacecraft collision avoidance challenge competition, in which the ML models were used to predict the final collision risk between orbiting objects. Li et al. [22] used the deep networks to estimate the final mass for the multitarget interplanetary missions with a mean relative error of less than 0.5% for low-thrust transfers and less than 4% for multi-impulse transfers. Peng et al. [23] used the artificial neural network to improve the orbit prediction accuracy. The simulation results show that the learning model could reduce prediction errors relative to physics-based models. Zhu et al. [24,25] used the deep neural network (DNN) to estimate the fuel consumption of the low-thrust transfers and perturbed long-duration impulsive transfers. Yang et al [26] proposed a DNN-based method to optimize the continuous low-thrust trajectory of the non-cooperative maneuvering spacecraft, and the method shows good generalization capacity of DNN. Chen et al. [27] developed the DNN to approximate the gravitational field of asteroids and a continuation approach was proposed to quickly optimize the time-optimal asteroid landing trajectories. Li et al. [28] used DNN to approximate the nonlinear functions in the actor-critic structure of the reinforcement learning method, which is employed to solve the optimal control problem of the switching system. For the manned lunar mission, the previous research shows that there is also a lack of recognition function or functional tool that can quickly evaluate and pattern recognize the lunar RD. For instance, it is required for the decision-maker to quickly and accurately evaluate whether an arbitrary lunar landing site is reachable. However, if the traditional trajectory optimization algorithm, e.g. the double two-body model, is employed to compute the RD by the traversal shooting strategy, the computation process would be extremely inefficient. The universal approximation theorem [29] states that the DNN has a good advantage of learning the underlying patterns and parameter characteristics of the model. As a result, this paper hopes to reveal the characteristics of the RD and approximate the coupling mechanism between the model parameters and the RD by the DNN. After the neural network is well trained, the obtained surrogate model can be applied to evaluating and calculating the RD in a quick way. The main innovations and contributions are listed as follows:

(i) The relationship between the RD at the perilune (PRL) and the orbit phase at the perigee is analyzed. It is the first time to identify that the RD of the FROs should be divided into eight types, and the orbit inclination and RAAN of the RD should be estimated individually.

(ii) Two surrogate models based on the DNNs are proposed, in which the CL model realizes the pattern recognition of the lunar RD and the RG model realizes the fast calculation of the lunar RD.

(iii) A serial design strategy is proposed by combining the trained CL and RG models for rapid analysis of the lunar RD. Moreover, a recognition tool is built in order to quickly judge whether an arbitrary lunar landing site is reachable.

The rest of the paper is organized as follows. Section 2 introduces the database-generation method of FROs. Section 3 defines the RD in the manned lunar mission and analyzes the characteristics of the RD of the FRO, which could provide a foundation for learning parameters selection of the DNN. Section 4 presents the whole implementation process in rapid analysis of RD via the DNN. The

CL and RG DNN are built to classify and calculate the lunar RD respectively. Section 5 gives the simulation examples and Section 6 draws the conclusions.

2. FRO optimization method

The orbit design and optimization method of the manned lunar exploration is the premise for the analysis of the RD. Due to the good symmetry of the "8" swing shape, the FRO has a natural advantage in safely returning the astronauts to the Earth and is usually used by the manned spacecraft. Therefore, the optimization of the FRO is introduced before RD analysis and the generation of the learning database.

If the time at the PRL t_{PRL}, and the corresponding Earth-centered J2000 (EJ2000) position $\boldsymbol{r}_{\mathrm{PRL}}^{\mathrm{EJ2000}}$ and velocity $\boldsymbol{v}_{\mathrm{PRL}}^{\mathrm{EJ2000}}$ are given, the FRO can be determined by forward and backward integration. Thus, in this paper the parameters $(t_{\mathrm{PRL}}, \boldsymbol{r}_{\mathrm{PRL}}^{\mathrm{EJ2000}}, \boldsymbol{v}_{\mathrm{PRL}}^{\mathrm{EJ2000}})$ are used to determine the FRO and the PRL parameters in the lunar sphere of influence (LSOI) are used to obtain $\boldsymbol{r}_{\mathrm{PRL}}^{\mathrm{EJ2000}}$ and $\boldsymbol{v}_{\mathrm{PRL}}^{\mathrm{EJ2000}}$ for the FRO design [11]. The selenocentric local-vertical-local-horizontal (LVLH) coordinate system $o_{\mathrm{M}} - x_{\mathrm{LVLH}} y_{\mathrm{LVLH}} z_{\mathrm{LVLH}}$ is introduced in Fig. 1, where the x-axis is the direction from geocentric to selenocentric, the y-axis is orthogonal to x-axis along the direction of the lunar motion and the z-axis forms a right-hand cartesian coordinate system with the other axes.

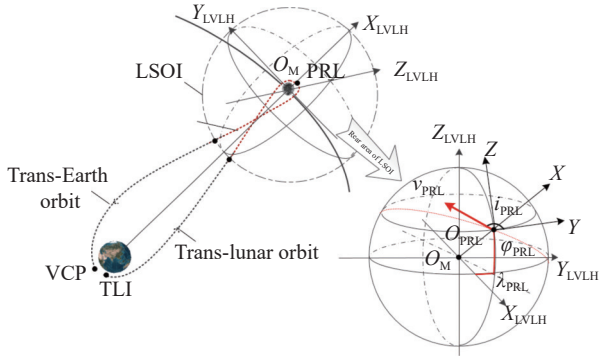

Fig. 1 Description of selenocentric LVLH coordinate and PRL coordinate

Then the PRL coordinate $o_{\mathrm{M}} - xyz$ is defined and the related parameters $\boldsymbol{\Phi}_{\mathrm{PRL}} = (\lambda_{\mathrm{PRL}}, \varphi_{\mathrm{PRL}}, v_{\mathrm{PRL}}, i_{\mathrm{PRL}})$ is called the pseudo PRL parameters. The angle i_{PRL} is the velocity azimuth angle and v_{PRL} is the PRL velocity. The angle λ_{PRL} and φ_{PRL} is the pseudo longitude and latitude of the PRL position. Rotate λ_{PRL} around the axis $o_{\mathrm{M}} - x_{\mathrm{LVLH}}$, and then rotate $-\varphi_{\mathrm{PRL}}$ around the axis y, and the PRL coordinate could be obtained.

Therefore, the direction of the PRL coordinate axes x, y, and z are determined according to the angle λ_{PRL} and φ_{PRL}, and the rotation relationship from the selenocentric LVLH coordinate to it. The origins of the two coordinate systems are both located at the Moon center. The conversion matrix from the PRL coordinate system to the LVLH coordinate system is formulated by

$$M_{\mathrm{PRL-LVLH}} = M_3(-\lambda_{\mathrm{PRL}}) \cdot M_2(\varphi_{\mathrm{PRL}}). \tag{1}$$

With the orbit height h_{PRL} given, the position and velocity in the PRL coordinate are $\boldsymbol{r}_{\mathrm{PRL}} = [h_{\mathrm{PRL}} + R_M, 0, 0]^{\mathrm{T}}$, and $\boldsymbol{v}_{\mathrm{PRL}} = [0, v_{\mathrm{PRL}} \cos i_{\mathrm{PRL}}, v_{\mathrm{PRL}} \sin i_{\mathrm{PRL}}]^{\mathrm{T}}$, and in the LVLH coordinate they are expressed by

$$\begin{cases} \boldsymbol{r}_{\mathrm{LVLH}} = M_{\mathrm{PRL-LVLH}} \cdot \boldsymbol{r}_{\mathrm{PRL}} \\ \boldsymbol{v}_{\mathrm{LVLH}} = M_{\mathrm{PRL-LVLH}} \cdot \boldsymbol{v}_{\mathrm{PRL}} \end{cases}. \tag{2}$$

Given the PRL time t_{PRL}, the Moon's inertial position $\boldsymbol{r}_{\mathrm{M}}^{\mathrm{EJ2000}}$ and velocity $\boldsymbol{v}_{\mathrm{M}}^{\mathrm{EJ2000}}$ can be interpolated by Jet Propulsion Laboratory (JPL) ephemeris, and the spacecraft's inertial states at PRL can be obtained by

$$\boldsymbol{r}_{\mathrm{PRL}}^{\mathrm{EJ2000}} = \boldsymbol{r}_{\mathrm{M}}^{\mathrm{EJ2000}} + \boldsymbol{r}_{\mathrm{LVLH}}, \tag{3}$$

$$\boldsymbol{v}_{\mathrm{PRL}}^{\mathrm{EJ2000}} = \boldsymbol{v}_{\mathrm{M}}^{\mathrm{EJ2000}} + \boldsymbol{v}_{\mathrm{LVLH}}. \tag{4}$$

Then the FRO could be determined by the backward and forward integration method. In order to describe the constraints of the FRO, the transfer process is divided into two phases: the trans-lunar orbit starting from the trans-lunar injection (TLI) to the PRL point, and the trans-Earth orbit starting from the PRL to the vacuum point (VCP) near the Earth, as shown in Fig. 1. The impulse at TLI is along the tangential direction of the velocity, and the TLI is the perigee of the geocentric launch phase. The orbit's RAAN and argument of latitude at TLI are adjustable. The inclination of the geocentric launch phase is restricted by the location of the launch site and the downrange angle of the rocket. The altitude of TLI is restricted by the carrying capacity of the rocket. Therefore, the constraint parameters of the trans-lunar orbit are the orbital height and inclination at TLI. As for the constraints of the trans-Earth phase, the reentry angle γ at the atmosphere entry time should be considered. With the atmospheric height h_{atmos} given, the tangent of the reentry angle γ could be obtained by

$$\tan\gamma = \frac{e_{\mathrm{reen}} \sin f_{\mathrm{reen}}}{1 + e_{\mathrm{reen}} \cos f_{\mathrm{reen}}} \tag{5}$$

where e_{reen} and f_{reen} are the eccentricity and true anomaly of the trans-Earth orbit at VCP, respectively.

The relationship between the VCP height and the reentry atmospheric height h_{atmos} is given by

$$r_{\mathrm{reen}} = \frac{r_{\mathrm{VCP}}(1 + e_{\mathrm{LSO}})}{1 + e_{\mathrm{LSO}} \cos f_{\mathrm{reen}}} = h_{\mathrm{atmos}} + R_{\mathrm{e}}. \tag{6}$$

By combining (5) and (6), the VCP height is expressed as

$$r_{\mathrm{VCP}}=\frac{1+\sqrt{1-(1-e_{\mathrm{reen}}^2)\sec^2\gamma}}{(1+e_{\mathrm{reen}})\sec^2\gamma}r_{\mathrm{reen}}. \tag{7}$$

Then the constraint of the reentry angle could be transformed into the constraint of the VCP height. Apart from the constraints above, the inclination of the return orbit should be also constrained because the distance of the reentry flight is limited by the reentry capacity of the lunar spacecraft. Therefore, the design variables of the FRO are $\boldsymbol{\Phi}_{\mathrm{PRL}}=(\lambda_{\mathrm{PRL}},\varphi_{\mathrm{PRL}},v_{\mathrm{PRL}},i_{\mathrm{PRL}})$, and the mission constraints include the orbit height and inclination of the trans-Earth phase and the trans-lunar phase, as given below:

$$\begin{cases}h_{\mathrm{TLI}}-h_{\mathrm{TLI}}^*=0\\ i_{\mathrm{TLI}}-i_{\mathrm{TLI}}^*=0\\ r_{\mathrm{VCP}}-r_{\mathrm{VCP}}^*=0\\ i_{\mathrm{VCP}}-i_{\mathrm{VCP}}^*=0\end{cases} \tag{8}$$

where the superscript $(\cdot)^*$ indicates the mission constraints.

The optimization of the FRO is a two-point value boundary problem and the numbers of the design variables and the constraints are equal to each other. Then, the sequential quadratic programming (SQP) algorithm is employed to solve the problem above [4].

3. Characteristics analysis of the lunar RD

3.1 Definition of the lunar RD

The decision-maker of the manned lunar mission mainly cares about whether the spacecraft could reach the target lunar site or whether the site is within the RD of the lunar orbit. The RD of the lunar orbit usually refers to the selenocentric longitudes and latitudes of the lunar surface region that can be reached by the orbits. Furthermore, the RD could also be defined as the domain of the characteristic parameters of the lunar orbit in high-dimension space. Given the initial time t_0 and the initial states $\boldsymbol{x}(t_0)\in\boldsymbol{\Theta}^n\subseteq\mathbf{R}^n$, if there is a control vector $\boldsymbol{u}(t)\in\boldsymbol{U}^m\subseteq\mathbf{R}^m$ resulting in the terminate state $\boldsymbol{y}(t_f)\in\boldsymbol{\Phi}^k\subseteq\mathbf{R}^k$ at the time t_f, the set $\boldsymbol{\Phi}^k$ is defined as the RD corresponding to the initial set $\boldsymbol{\Theta}^n$ by

$$\begin{cases}\dot{\boldsymbol{x}}(t)=f[t,\boldsymbol{x}(t),\boldsymbol{u}(t)]\\ \boldsymbol{y}(t)=c[t,\boldsymbol{x}(t)]\\ \boldsymbol{x}(t_0)\in\boldsymbol{\Theta}^n,\boldsymbol{u}(t)\in\boldsymbol{U}^m,\boldsymbol{y}(t_f)\in\boldsymbol{\Phi}^k\\ f(\cdot):\boldsymbol{\Theta}^n\times\boldsymbol{U}^m\to\boldsymbol{\Theta}^n\\ c(\cdot):\boldsymbol{\Theta}^n\to\boldsymbol{\Phi}^k\end{cases} \tag{9}$$

where $\boldsymbol{y}(t)=c[t,\boldsymbol{x}(t)]$ is a nonlinear function of t and $\boldsymbol{x}(t)$. The RD $\boldsymbol{\Phi}^k\subseteq\mathbf{R}^k$ could be obtained by $\boldsymbol{y}(t_f)$. In this paper, the orbital inclination i_{PRL} and RAAN Ω_{PRL} at the PRL is used to describe the RD as

$$\boldsymbol{\Phi}^k=(i_{\mathrm{PRL}},\Omega_{\mathrm{PRL}}). \tag{10}$$

The two characteristic parameters i_{PRL} and Ω_{PRL} describe the direction of the orbit plane at the PRL. When i_{PRL} and Ω_{PRL} are given, the sub-satellite point of the lunar orbit is calculated by orbit propagation, and the reachable region of the lunar surface could be further obtained.

3.2 Analysis of RD characteristics

The lunar RD is defined in (10) and then the set of the FRO is generated to analyze the variation features of the RD, which would provide a reference for the feature selection of the deep learning model. For the mission constraints in (9), the TLI height is set as $h_{\mathrm{TLI}}=170$ km which is similar to the Apollo mission [30]. The TLI inclination is set as $i_{\mathrm{TLI}}=28^\circ$, which considers the motion of the Moon and the orbital transfer window [4]. According to the practical engineering constraints [31], $e_{\mathrm{reen}}=0.97$, $\gamma=-6^\circ$, the Earth radius is $R_{\mathrm{E}}=6\,378.137$ km, the atmospheric altitude is $h_{\mathrm{atmos}}=122$ km, and then the VCP height $h_{\mathrm{VCP}}=50$ km can be obtained by (6) and (7). Considering the Earth land-return mission, the VCP inclination constraint is set by $i_{\mathrm{VCP}}=42^\circ$. In order to properly describe the RD of the FRO, it is divided into four types, i.e., "I", "II", "III", and "IV", according to the orbital phase at TLI and VCP. It is also labeled by "0" and "1" according to the orbit phase at PRL. Thus, the RD is divided into eight types in total as shown in Table 1.

Table 1 CL of eight orbit types of FRO

Type	Name	TLI phase	VCP phase	PRL phase
I	I-0	Ascending	Ascending	Ascending
	I-1	Ascending	Ascending	Descending
II	II-0	Ascending	Descending	Ascending
	II-1	Ascending	Descending	Descending
III	III-0	Descending	Ascending	Ascending
	III-1	Descending	Ascending	Descending
IV	IV-0	Descending	Descending	Ascending
	IV-1	Descending	Descending	Descending

The PRL altitude is $h_{\mathrm{PRL}}=100$ km. The mission epoch is required between 2029-04-01 00:00:00 and 2029-05-01 00:00:00. By applying the trajectory design method in Section 2, different types of FROs are generated. The nonlinear and graphic characteristics of the PRL inclination and RAAN of the RD are demonstrated in Fig. 2 and Fig. 3.

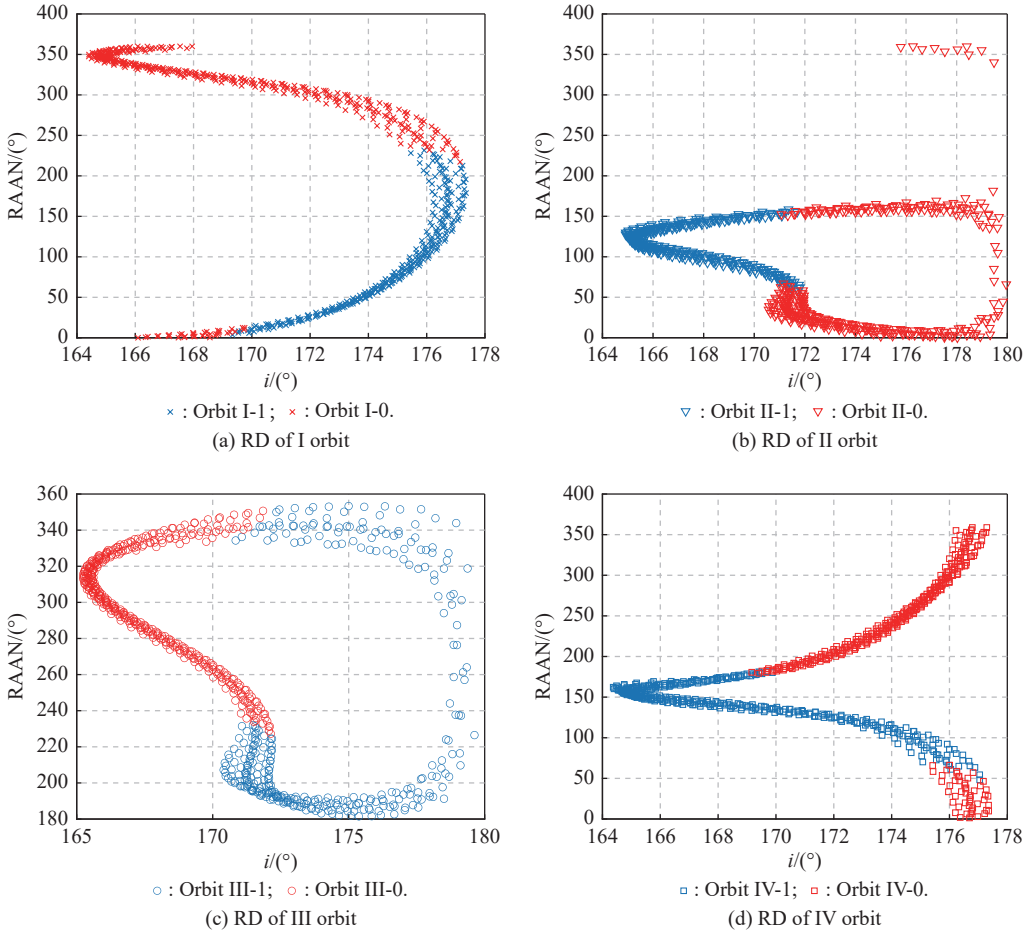

Fig. 2 RD of different types of FROs in LCF coordinate

From Fig. 2(a) it can be found that the RAAN of the type "I" RD in the lunar-centered fixed (LCF) coordinate varies from 0° to 360°, meaning full access to the lunar surface along the selenocentric longitude. The inclination is approximately from 164.2° to 177°. The relationship between the RAAN and inclination of the "I" type RD is approximately distributed as a curve of "S" shape. Besides, the RDs of the type "I-0" (red parts) and "I-1" (blue parts) are independent from each other without overlapping parts.

For the type "II" RD in Fig. 2(b), the PRL RAAN is mainly between 0° and 180°, and a small amount of points appear around 360°. The PRL inclination varies from 165° to 180°. The nonlinear relationship between the inclination and RAAN is not "one-to-one" and the shape of the "II" RD looks like a reclining "tooth".

For the type "III" RD in Fig. 2(c), the PRL RAAN also has full lunar access along the selenocentric longitude with a range from 0° to 360°. The curve of the RAAN and inclination is plotted as a "heart" shape.

For the type "IV" RD in Fig. 2(d), the relationship of the RAAN and inclination is interesting, which looks like a rotating "peak" shape. The RAAN of the type "IV" also has full access to the Moon surface.

Especially, for all the "I", "II", "III" and "IV" RDs, the orbit phase "0" (the red parts) or "1" (the blue parts) at the PRL does not overlap each other. It means that for a specific inclination and RAAN, there is only one solution to the arrival phase at the PRL.

The RDs of all the eight types of FROs are all plotted in Fig. 3.

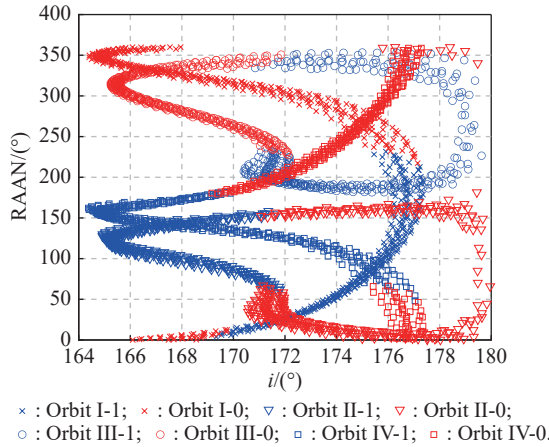

Fig. 3 Whole RD of four types of FROs in LCF coordinate (plotted in one map)

The orbits of "I" and "IV" types have a full access to the Moon surface along the selenocentric longitude, while the ranges of the "II" and "III" types mainly lies between 0° and 180°. A small amount of the RAANs of the "III" type orbits locate between 340° and 360°. Besides, the "III" RD could be approximately seen as a translation transformation of the "II" RD.

The above characteristics analysis of the FRO's RD show that different types of FROs have different nonlinear relationships between the RAAN and the inclination. The graphic structure of the RD's inclination and RAAN also demonstrates different interesting features.

In the following, the deep learning method is used to excavate and approximate the underlying patterns of the RD of FROs.

4. Evaluating RD based on deep learning method

The reachable regions of the lunar surface could be known quickly with the FRO's RD, which provided a reference for the overall engineering decision making. The characteristics above show that different orbits have different types of the RD at the PRL time. Moreover, the mission constraints such as the orbit phase at the PRL also has an important effect on the topological structure of the graphic curve of the inclination and RAAN. The database of FROs is designed and generated, then the DNN is applied to approximating and calculating the RD.

4.1 Database generation

The learning database of FROs is generated and the simulation parameters are listed in Table 2. The orbit inclination and height constraints at TLI are $i_{\mathrm{LEO}} = 28° \pm 2°$ and $h_{\mathrm{LEO}} = 170$ km. The constraints at VCP are $i_{\mathrm{VCP}} = 42° \pm 2°$ and $h_{\mathrm{VCP}} = 50$ km. The PRL height is set by $h_{\mathrm{PRL}} = 100$ km and the mission epoch is limited within three months which starts from 2029-04-01 00:00:00 to 2029-07-01 00:00:00. The ascending phase and descending phase at the PRL and TLI are both considered. 87 261 FROs are generated, in which the percentage of 70%, 15%, 15% are labeled by training sets, testing sets and verifying sets respectively.

Table 2 Ranges of the orbit learning database of FROs

Parameter	Range
i_{LEO}/(°)	26−30
i_{VCP}/(°)	40−44
h_{LEO}/km	170
h_{VCP}/km	50
T_{Transfer}/day	5.5−6.0
t_{PRL}	2029-04-01 00:00:00−2029-07-01 00:00:00
TLI phase	Ascending, Descending
PRL phase	Ascending, Descending
VCP phase	Ascending, Descending

In order to well approximate the RD of FROs, it is necessary to recognize the types of the RD correctly because the RD of eight types of orbits has a completely different graphic characteristics as demonstrated in Fig. 3. The surrogate model of CL should be built to correctly classify the type of the orbit and recognize the pattern of the RD, which is a prerequisite for calculating the RD. Then, with the orbit type known, the surrogate model of RG is trained to quickly analyze the characteristics and the nonlinear relationship of the orbit RAAN and inclination at the PRL, and to calculate them as well. In the following part, the learning features selection and the training methods are introduced for both the CL and RG neural networks.

4.2 Learning features selection

For the deep learning problem studied in this paper, the combination of learning features has an important effect on the learning performance and based on the domain knowledge, we could select the appropriate orbital features that obviously affect the learning effect and combine the selected features as the input of the DNN. Due to the quasi-symmetry of the FRO, when the spacecraft flies in the cislunar space and arrives at the Moon, the distribution of the inclination and RAAN at the PRL is mainly affected by the relative position between the Earth and the Moon at the PRL time. For instance, the relationship between the PRL phase of "I" FRO and the argument of latitude u_{m} of the Lunar orbit is plotted in Fig. 4. It can be found that the spacecraft in the FRO arrives at PRL in the ascending phase when the u_{m} locates between 100° and 260°, and the spacecraft arrives in the descending phase when the u_{m} falls in the other degree intervals. The argument of latitude has an obvious effect on the orbital phase at PRL.

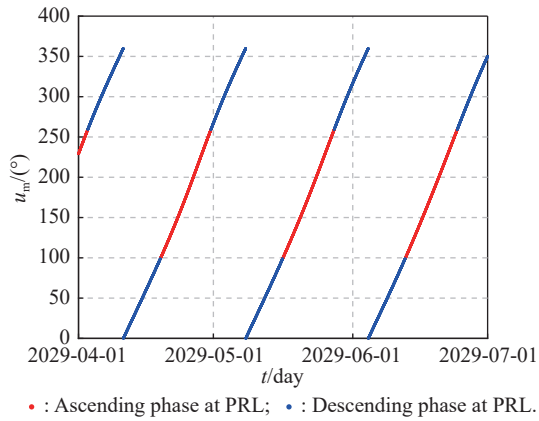

Fig. 4 Ascending and descending phases vs time and lunar argument of latitude

As a result, the argument of latitude of the lunar orbit can be used as the input of the DNN. In fact, the lunar

orbit around the Earth is an ellipse and the other orbital elements are also used as the learning features, which is listed in Table 3.

Table 3 Learning features of the CL model

Name	Variable
Semi-major axis	a_{M}
Eccentricity	e_{M}
Inclination	i_{M}
RAAN	Ω_{M}
Argument of latitude	u_{M}

Therefore, the first surrogate model for CL is mathematically modeled as follows:

$$\mathrm{Net}_{\mathrm{CL}}(\theta):\boldsymbol{R}_{\mathrm{CL}}^{\mathrm{Input}}\rightarrow\boldsymbol{R}_{\mathrm{CL}}^{\mathrm{Output}} \tag{11}$$

where $\boldsymbol{R}_{\mathrm{CL}}^{\mathrm{Input}}=(a_{\mathrm{M}},e_{\mathrm{M}},i_{\mathrm{M}},\Omega_{\mathrm{M}},u_{\mathrm{M}})$ is the input of the neural network, θ is the network parameter, $\boldsymbol{R}_{\mathrm{CL}}^{\mathrm{Output}}=$ ("TYPE") is the output of the neural network including the orbit type of "ascending phase" and "descending phase".

The inclination and RAAN of the RD at the PRL are also influenced by the relative position between the Moon and the Earth, and the orbital elements of the Moon's orbit are chosen as the input features of the RG model, which is used for quickly calculating the RD. Besides, the RD is influenced by the mission constraint such as the departure orbit height and inclination at TLI, returning orbit height and inclination at VCP, and these parameters should be used as the input of the neural network as well. The learning features of the RG network is summarized in Table 4.

Table 4 Learning features of the RG model

Name	Variable
Semi-major axis	a_{m}
Eccentricity	e_{m}
Inclination	i_{m}
RAAN	Ω_{m}
Argument of latitude	u_{M}
LTO height	h_{LEO}
LTO inclination	i_{LEO}
PRL height	h_{PRL}
VCP inclination	i_{VCP}
VCP height	h_{VCP}

And it is mathematically modeled as follows:

$$\mathrm{Net}_{\mathrm{RG}}(\theta):\boldsymbol{R}_{\mathrm{RG}}^{\mathrm{Input}}\rightarrow\boldsymbol{R}_{\mathrm{RG}}^{\mathrm{Output}} \tag{12}$$

where $\boldsymbol{R}_{\mathrm{RG}}^{\mathrm{Input}}=(a_{\mathrm{M}},e_{\mathrm{M}},i_{\mathrm{M}},\Omega_{\mathrm{M}},u_{\mathrm{M}},h_{\mathrm{LEO}},i_{\mathrm{LEO}},h_{\mathrm{PRL}},h_{\mathrm{VCP}},i_{\mathrm{VCP}})$ is the input of the RG network, θ is the network parameters and $\boldsymbol{R}_{\mathrm{RG}}^{\mathrm{Output}}=\boldsymbol{\Phi}^{\mathrm{k}}=(i_{\mathrm{PRL}},\Omega_{\mathrm{PRL}})$ is the RD at PRL and is also the output of the network.

4.3 Neural network training

There are many types of DNNs, such as fully connected neural networks, convolutional neural networks, long and short memory neural networks, and so on [24]. For the CL and RG problem in this paper, the fully connected neural network is enough to approximate the nonlinear characteristics of the RD. Thus, the fully connected neural network is chosen to solve the learning problem in this paper. The structure of the fully connected neural network is composed of three parts: the input layer, the output layer, and the hidden layer. The input layer or the output layer is composed of the nodes, the number of which is determined by the learning features and the learning results respectively. The structure of the hidden layer includes the number of layers and the number of nodes in each layer. The data is transmitted between nodes in each layer and the activation of a node can be seen as the summation of all the weighted inputs, which is expressed as

$$x_i=f_i\left(\sum_{j=1}^{N}\omega_{ij}x_j+b_i\right) \tag{13}$$

where x_j is the output of the node in the previous layer, x_i is the output of the current layer, ω_{ij} is the weight factor from node i to node j, b_i is the variable bias of the node i, N is the number of the nodes in the previous layer, and f_i is the activation function.

Equation (13) indicates that the output of the previous layer is the input of the current layer. The network training can be regarded as a process to adjust the weight factors and minimize the loss function.

For the CL network, the cross-entropy is employed as the loss function and it is formulated by

$$L=-\frac{1}{N}\sum_{i=1}^{N}\sum_{c=1}^{M}y_{ic}\lg p_{ic} \tag{14}$$

where N is the number of the training samples, M is the number of the CL categories, y_{ic} is the label of the training data, and p_{ic} is the predicted CL probability by the network.

For the RG network, the mean square error (MSE) function is used as the loss function, and is expressed by

$$\mathrm{MSE}=\sqrt{\frac{1}{N}\sum_{i=1}^{N}(\hat{x}_i-x_i)^2} \tag{15}$$

where N is the number of the training samples, $\hat{x}_i$ is the predicted value by the network, and x_i is the true value of the training data.

Meanwhile, the mean absolute error (MAE) function is also used as the RG network's evaluation function, which is formulated by

$$\text{MAE} = \frac{1}{N}\sum_{i=1}^{N}|\hat{x}_i - x_i|. \tag{16}$$

4.4 Implementation process

It should be noted that the similarity between the CL and RG neural networks is that they both employ the full-connection neural network as the learning surrogate model. The differences between the two training methods are listed as follows. Firstly, the CL neural network uses the cross-entropy as the loss function, while the RG neural network uses the MSE function. Secondly, the tuning results of the two network's hyperparameters and training methods are different and they will be demonstrated in the numerical simulation. Moreover, after the two neural networks being well-trained, a serial strategy is proposed to combine them for quick RD analysis and a recognition tool is built to assess whether the lunar site can be reached, which is described in Fig. 5 and Fig. 6 respectively.

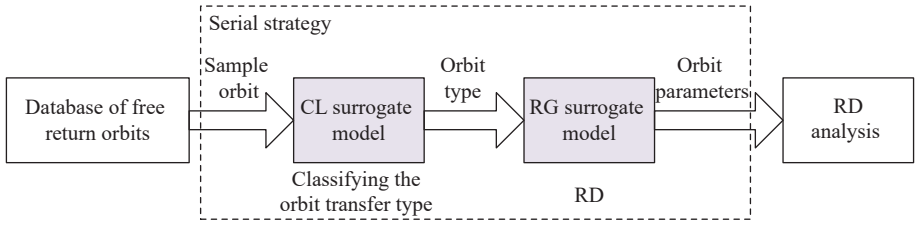

Fig. 5 Description for serial strategy

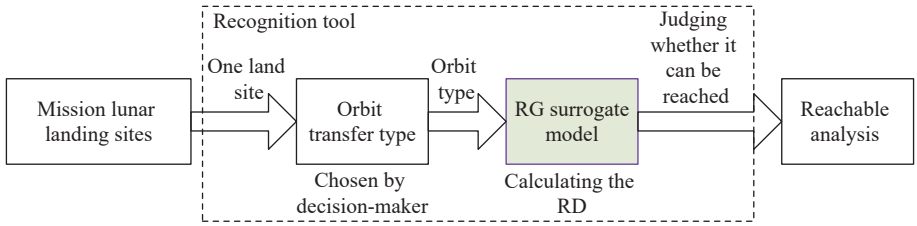

Fig. 6 Implementation process of recognition tool

For the serial strategy, if a sample FRO is given, the surrogate model of CL is firstly used to estimate the orbit type of the RD. Because different types of RD have different topological characteristics and then it helps choose the appropriate surrogate model of RG to quickly calculate the orbit inclination and RAAN at the PRL.

The other application of the surrogate model is to build a recognition tool to assess whether a lunar site can be reached. The target lunar landing site is selected from the candidate landing sites that is required by the mission, and the decision-maker chooses the concerned orbit transfer type. Then the corresponding RG surrogate model is used to quickly generate the orbit's RD and assess whether the target site could be reached by the orbit. For instance, if the position of the site could be overlapped by the RD in the map, it is concluded that the site can be reached.

Therefore, the total process of quickly evaluating the RD via the DNN is illustrated in Fig. 7 and it is described as follows. Firstly, the trans-lunar database of FROs is generated according to the mission constraints and the epoch, which includes the types of the RD and the corresponding inclination and RAAN at the PRL.

The generated database used for the CL neural network training is divided into four types of FROs: "I", "II", "III", and "IV". And four CL models are trained to evaluate the ascending or the descending phase of the RD at the PRL. As for the orbit database used for the RG network training, it contains eight types of FROs that further consider the PRL orbit phase: I-0, I-1, II-0, II-1, III-0, III-1, IV-0 and IV-1. Thus, eight RG models should be trained corresponding to the eight types of RD.

Then the CL neural network and the RG neural network are trained respectively. When training the CL neural network, the loss function of cross-entropy is used, and the ascending phase and the descending phase is the output of the neural network for the eight types of the generated CL database. And for the RG network training,

the MSE loss function is used and the inclination and RAAN at the PRL is the output of the neural network. The selection of the two neural network's hyperparameters and the learning performance of the two models are also discussed.

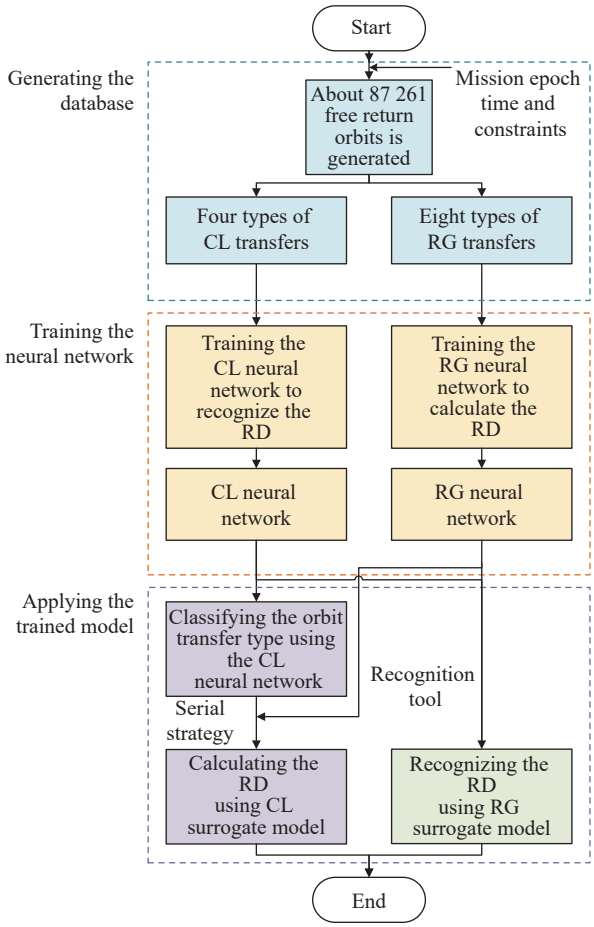

Fig. 7 Whole process of the RD analysis for the manned lunar mission

After being well trained, the two neural networks or surrogate models are applied to quickly analyzing the RD of the manned lunar mission. A serial strategy is proposed to evaluate the RD in a quick way, where the surrogate model of CL is firstly used to estimate the orbit type of the RD and then the surrogate model of RG is secondly used to calculate the orbit inclination and RAAN at the PRL. Moreover, a recognition tool is built in order to judge whether an arbitrary lunar landing site is reachable in a quickly and accurately way. The Monte Carlo simulation is conducted to verify the correctness of the proposed method.

5. Numerical simulation

In this paper the mission epoch of China's manned lunar mission is set in 2029. The computer processor is Intel Core i7-7700 CPU 3.60 GHz. The RAM is 8.00 GB, and the desktop system is Windows 10.

5.1 Hyperparameter tuning of neural network

The candidate hyperparameters of the CL and RG neural networks are listed in Table 5. The training optimizers include the stochastic gradient descent (SGD), the Adam, the Nadam and the Levenberg-Marquarelt (LM). The activation function in the hidden layer includes the sigmoid, the softsign, the tanh and the ReLU function, and the number of the hidden layers is set from 1 to 4. The learning rate is limited between 0.000 01 and 0.1. Note that when the learning rate is too large, it is easier for the trained model to converge but it is more possible to fall into a local optimum. On the other hand, a too small learning rate makes the neural network difficult to converge.

Table 5 Search ranges of the hyperparameters for both the CL and RG models

Hyperparameter	Search range
Optimizer	SGD, Adam, Nadam, LM
Activation function	sigmoid, softsign, tanh, ReLU
Number of layers	[1,4]
Number of nodes	[8, 128]
Learning rate	[0.000 01, 0.1]

The tuning results of the suitable hyperparameters of the two neural networks and the suggested configurations are listed in Table 6. Both of the two training models have two hidden layers. The number of the neural nodes is 8 and 16 for the CL model, and it is 16 and 32 for the RG model. The optimizers are selected by the Adam and LM algorithm for the two networks and the activation functions in the hidden layers are the tanh function and the ReLU function, respectively. A small learning rate of 0.005 is preferred when training both the CL and RG neural networks.

Table 6 Tuning results of the hyperparameters for both the CL and RG models

Hyperparameter	CL model	RG model
Optimizer	Adam	LM
Activation	tanh	ReLU
Number of layers	2	2
Number of nodes	[8,16]	[16, 32]
Learning rate	0.005	0.005

5.2 Performance of the neural network

5.2.1 CL model for evaluating RD

Four CL models are learned in order to evaluate the type of the RD. The learning performance of the MSE, CL accuracy, total training number, and training time of the four CL models are summarized as in Table 7. The learned result indicates that the obtained surrogate model could approximate the RD's underlying patterns well. This is because in the above analysis, the ascending and descending orbital phases of each type of FROs are obviously affected by the argument of latitude of the lunar orbit around the Earth. This paper takes the lunar orbital elements as the learning feature input based on the domain knowledge, so the CL model has a good CL accuracy. The CL results verify the correctness of the selected learning features in turn.

Table 7 Learning results for the four CL models

Orbit type	MSE	Accurate number	Total number	Accuracy rate/%	Training time/s
I	$4.510\,8\times10^{-4}$	21 797	21 803	99.97	306
II	0.002 2	21 810	21 822	99.95	355
III	$4.085\,6\times10^{-4}$	21 808	21 812	99.98	327
IV	0.001 831	21 813	21 824	99.95	317

The learning error histograms of the four models are shown in Figs. 8−11. The histogram errors are mainly distributed at [−0.034 62, 0.034 62], [−0.087 78, 0.087 78], [−0.037 58, 0.037 58] and [−0.084 14, 0.084 14] respectively. The histograms are symmetrically distributed along the horizontal axis, which also verify the correctness of the selection of the model hyperparameters.

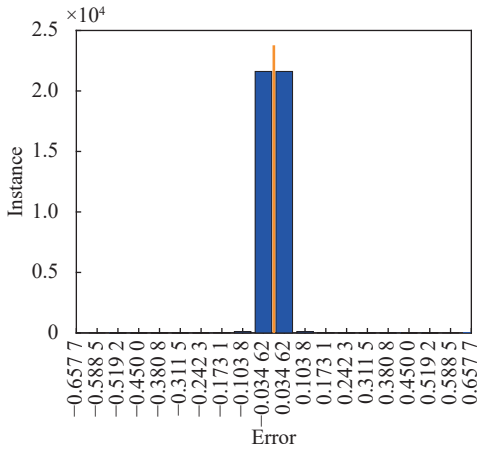

Fig. 8 Learning error histogram of CL model I

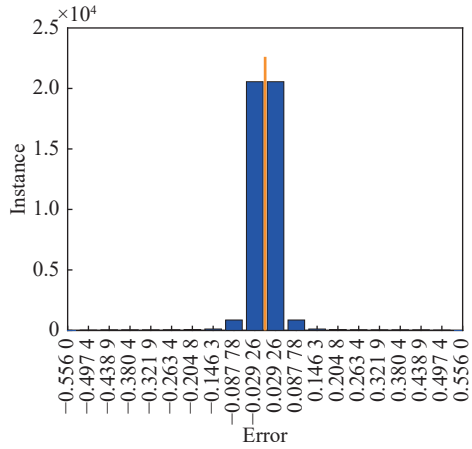

Fig. 9 Learning error histogram of CL model II

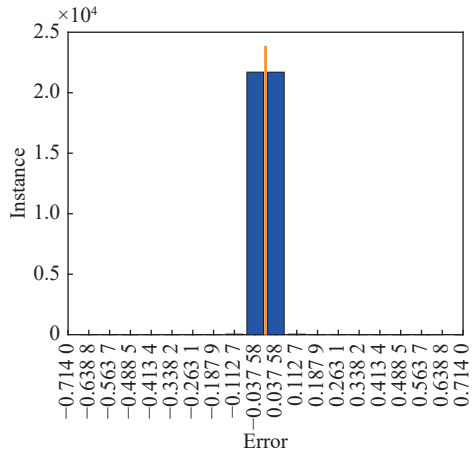

Fig. 10 Learning error histogram of CL model III

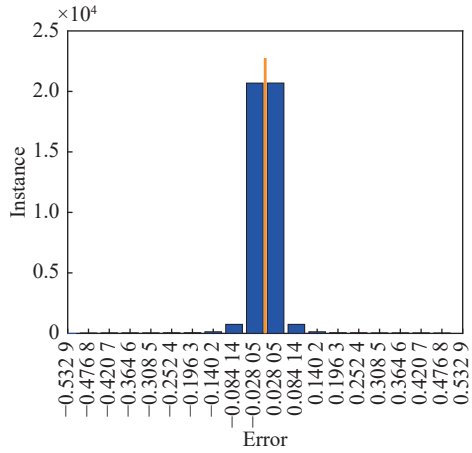

Fig. 11 Learning error histogram of CL model IV

5.2.2 RG model for calculating RD

For the four types of FROs, each type of the orbit is

labeled according to the ascending or descending orbit phase at the PRL, and a total of eight RG models are generated to calculate the orbit inclination and RAAN of the RD. The learning performance is shown in Table 8. It can be found that the training time increases compared with the CL model, and most of the model's training time is more than eight minutes. The difference in the CL and RG models' training time is determined by the problem characteristics. According to the orbit characteristic analysis in this paper, the CL neural network is built according to the orbit types that is discrete, but the RG neural network is constructed to solve the continuous problem, in which the inclination and RAAN have a range of $[0°, 180°]$ and $[0°, 360°]$, respectively. Therefore, it is more difficult to learn the RG characteristics of the RD than the CL characteristics.

Table 8 Learning results for the four RG models

Orbit type	Inclination MSE/(°)	RAAN MSE/(°)	Inclination MAE/(°)	RAAN MAE/(°)	Training time/s
I-0	1.635×10^{-5}	2.858×10^{-4}	5.665×10^{-4}	1.518×10^{-3}	553
I-1	9.178×10^{-5}	1.103×10^{-4}	6.532×10^{-3}	7.504×10^{-3}	373
II-0	1.646×10^{-6}	1.848×10^{-4}	7.052×10^{-4}	1.439×10^{-3}	523
II-1	2.524×10^{-5}	3.586×10^{-4}	2.888×10^{-3}	4.880×10^{-3}	461
III-0	1.939×10^{-5}	3.733×10^{-3}	3.093×10^{-3}	7.864×10^{-3}	528
III-1	4.845×10^{-6}	4.850×10^{-4}	1.394×10^{-3}	2.708×10^{-3}	545
IV-0	4.024×10^{-5}	1.930×10^{-4}	5.102×10^{-3}	8.275×10^{-3}	542
IV-1	8.532×10^{-5}	1.277×10^{-4}	7.337×10^{-3}	6.591×10^{-3}	535
Average	3.560×10^{-5}	6.848×10^{-4}	3.452×10^{-3}	5.128×10^{-3}	507.5

The performance of the RG neural network is shown in Figs. 12−15, and all the eight obtained RG models are well trained with acceptable learning errors. For the learning error of the inclination at the PRL, the minimum MSE is 1.646×10^{-6} (Model II-0) and the maximum MSE is 9.718×10^{-5} (Model I-1). For the model performance of the RAAN, the minimum MSE is 1.103×10^{-4} and the maximum is 3.733×10^{-3}. The learning error of RAAN is generally greater than that of orbital inclination because the two orbit variables have different ranges. The orbital inclination varies from 0° to 180° and the RAAN varies from 0° to 360°. The histograms of the inclination and RAAN's MSEs are shown in Fig. 12 and Fig. 13, respectively.

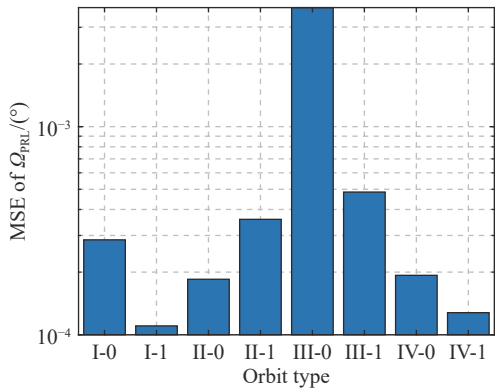

Fig. 13 MSEs of RAAN of eight RG models

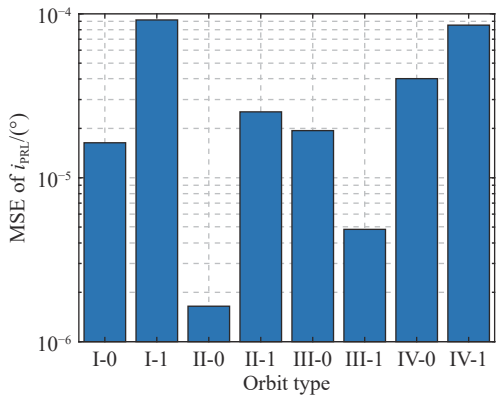

Fig. 12 MSEs of inclination of eight RG models

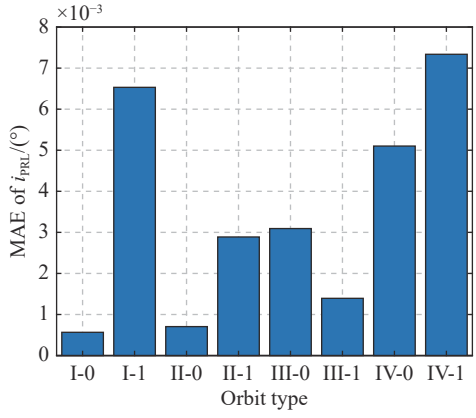

Fig. 14 MAEs of inclination of eight RG models

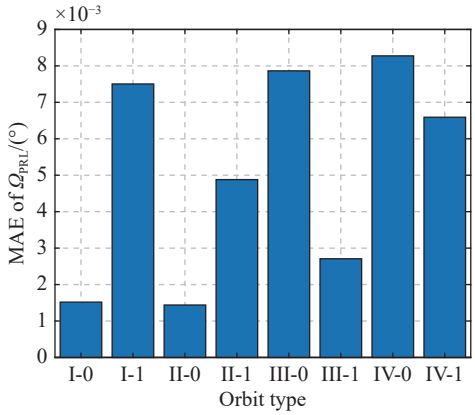

Fig. 15 MAEs of RAAN of eight RG models

For the MAE of the two variables, the minimum MAE of the inclination is 5.665×10^{-4}, and the maximum is 7.337×10^{-3}. For the MAE of the RAAN at the PRL, the minimum value is 1.439×10^{-3}, and the maximum value is 7.864×10^{-3}. The average MSE and average MAE of the RD's inclination and RAAN are 3.560×10^{-5}, 6.848×10^{-4}, 3.452×10^{-3}, and 5.128×10^{-3}, respectively. The histograms of the inclination and RAAN's MAEs are shown in Fig. 14 and Fig. 15, respectively.

5.3 Application in manned lunar mission design

In the following part, the trained deep learning model is applied to the RD analysis of the manned lunar mission, and the generalization ability of the learning model is also verified. The selected mission window is set from July 1 2029 to August 1 2029, and 875 FROs are randomly generated. Based on the proposed serial strategy, the CL surrogate model is firstly used to recognize the type of the RD. And 874 orbits are correctly judged, the accuracy is more than 99%. Secondly, the RG surrogate model is applied to estimating the orbit inclination and RAAN of the RD at the PRL, and the MAEs are 0.001 710° and 0.038 715°, respectively. It is worth noting that although there are some learning errors in the obtained neural network, the calculation time of the surrogate model is very short after it is well trained. For the 875 orbits in this paper, the calculation time is about 0.153 2 s. If the traditional optimization based on the double two-body model is adopted, the calculation time of a single orbit is about 4.94 s and the overall calculation time is about 1.2 hours and the results are compared in Table 9.

Table 9 Comparison of the computation time between two models

s

Computation time	Deep learning model	Double two-body model
Total time	0.153 2	4 322.5
Computation time per orbit	1.7509×10^{-4}	4.94

Moreover, if the numerical method based on the high-fidelity model is used, the computation time would be much longer. Therefore, the RG model and the CL model based on DNN learning have a good advantage in computation efficiency when the trained model is used for the analysis of the RD of the manned lunar mission.

Finally, in order to further verify the correctness of the obtained surrogate model proposed in this paper, the CL model and the RG model is combined with each other, and a recognition and estimation tool of the RD is built in order to quickly judge whether an arbitrary lunar landing site could be reached. A total of 10 000 global lunar landing sites are randomly generated, and the RD of "I" FRO is considered. The Monte Carlo simulation results are depicted in Fig. 16.

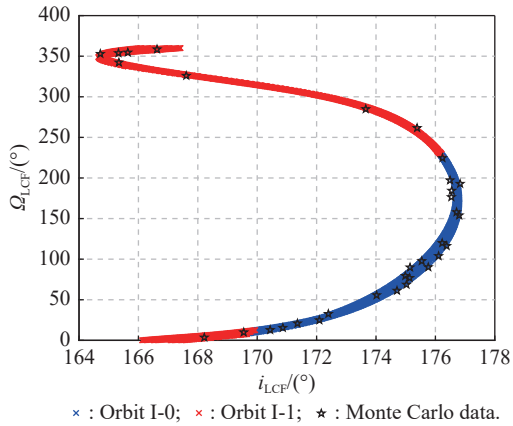

Fig. 16 Simulation results of the 10 000 randomly generated sites

It is shown that about 37 of the 10 000 generated sites can be "reached", where the reachable sites are located in the PRL RD graph of I-0 and I-1 FROs. The orbit inclinations and RAANs of 10 reachable sites are listed in Table 10 and the differences between the result of the deep learning model and the traditional optimization method based on the double two-body model are also compared.

Table 10 Difference in the geocentric position of the recognition tool and the landing site

(°)

Number	Method					
	Monte Carlo data		PRL method		DNN method	
	Ω_{LCF}	i_{LCF}	Ω_{LCF}	i_{LCF}	Ω_{LCF}	i_{LCF}
1	176.71	157.96	176.71	157.95	176.71	157.95

Continued

Number	Method					
	Monte Carlo data		PRL method		DNN method	
	Ω_{LCF}	i_{LCF}	Ω_{LCF}	i_{LCF}	Ω_{LCF}	i_{LCF}
2	174.99	79.42	174.98	79.41	174.98	79.41
3	165.33	353.87	165.34	353.87	165.35	353.87
4	170.44	12.82	170.44	12.81	170.44	12.84
5	170.86	15.49	170.85	15.49	170.85	15.49
6	176.24	224.62	176.25	224.64	176.24	224.64
7	171.35	20.92	171.35	20.94	171.36	20.94
8	175.54	97.67	175.57	97.65	175.57	97.65
9	174.02	55.67	173.98	55.69	173.98	55.69
10	176.23	119.92	176.22	119.97	176.22	119.97

On the one hand, the Monte Carlo shooting data is nearly the same to the generated RD graph, meaning that the selected sites are reliably reachable. And the shooting sites are also consistent with the RD data predicted by the deep learning model. Therefore, the Monte Carlo simulation proves that such a RD recognition and estimation tool built by the DNN is a feasible idea, and it can be used for calculating the RD with acceptable errors. On the other hand, the computation time of the Monte Carlo simulation via the DNN is 2.013 3 s. However, if the optimization method by pseudo PRL parameters is used to traverse the scatter points of the RD and then to judge the intersection relationship between the RD graph and the target site, the simulation process is very time-consuming, which would consume more than tens of hours. Therefore, the proposed method to estimate the RD of the FRO can not only be used for quickly calculating RD, but also be used to build a recognition tool for judging whether a given target lunar site is reachable. They both show the advantage of the proposed method in computation efficiency.

6. Conclusions

In this paper, a fast calculation method of the RD of manned lunar FROs via deep neural network is proposed. The RD of the manned lunar mission is defined, and the RD database is generated based on the FRO optimization method using pseudo PRL parameters. The nonlinear characteristics between the inclination and RAAN of eight different types of FROs at the PRL are analyzed in the two-dimensional graphic structure of the RD. Then, two neural networks are built, in which the classification model is used for recognize the type of the RD and the RG model is used to calculate the inclination and RAAN of the RD. The simulation results show that the obtained surrogate model could classify the RD with the accuracy of more than 99%, and could also estimate the inclination and RAAN at PRL with the error of less than 0.01°. The obtained surrogate models show the advantage in computation efficiency that its computation cost is much less than the traditional optimization method based on the double two-body model. In order to apply the trained models, a rapid recognition tool is built for quickly judging whether an arbitrary lunar landing site is reachable, which can provide reference and support for the overall decision-making of manned lunar landing missions in the future.

References

[1] DUGGAN M, SIMON X, MOSEMAN T. Lander and cislunar gateway architecture concepts for lunar exploration. Proc. of the IEEE Aerospace Conference, 2019. DOI: 10.1109/AERO.2019.8741766.

[2] HAN L. NASA updates the artemis mission. Chinese Journal of Space Science, 2020, 40(6): 967–967. (in Chinese)

[3] QIAN Y Q, XIAO L, HEAD J W, et al. Young lunar mare basalts in the Chang'e-5 sample return region, northern Oceanus Procellarum. Earth and Planetary Science Letters, 2021, 555: 116702.

[4] YANG L Y, ZHANG J, LI H Y, et al. Design and characteristic analysis for land module's trans-lunar trajectory based on multi-conic method. Journal of Astronautics, 2019, 40(12): 1383–1392. (in Chinese)

[5] ZHENG A W, ZHOU J P. A survey on trajectory design and constrains of manned lunar landing missions. Manned Spacecraft, 2012, 18(1): 48–54. (in Chinese)

[6] PENG K, YANG L. Analysis on human lunar exploration flight modes via cislunar space station. Journal of Astronautics, 2018, 39(5): 471–481. (in Chinese)

[7] TOPPUTO F. On optimal two-impulse Earth–Moon transfers in a four-body model. Celestial Mechanics and Dynamical Astronomy, 2013, 117(3): 279–313.

[8] LYU M B, TAN M H, ZHOU D M. Design of two-impulse Earth–Moon transfers using differential correction approach. Aerospace Science and Technology, 2017, 60: 183–192.

[9] GAO Y F, WANG Z K, ZHANG Y L. Analytical design methods for transfer trajectories between the Earth and the Lunar orbital station. Astrophysics and Space Science, 2018,

363: 206.
[10] MIELE A. Theorem of image trajectories in the Earth-Moon space. Astronautica Acta, 1960, 6(51): 225–232.
[11] ZHOU W M, LI H Y, HE B Y, et al. Fixed-thrust Earth–Moon free return orbit design based on a hybrid multi-conic method of pseudo-perilune parameters. Acta Astronautica, 2019, 160: 365–377.
[12] LUO Q Q, YIN J, HAN C. Design of Earth-Moon free-return trajectories. Journal of Guidance, Control, and Dynamics, 2013, 36(1): 263–271.
[13] WEN C X, ZHAO Y S, SHI P. Precise determination of reachable domain for spacecraft with single impulse. Journal of Guidance, Control, and Dynamics, 2014, 37(6): 1767–1779.
[14] PENG Q B. Optimal trajectory design and characteristics analysis for manned lunar landing mission with emergency return capability. Changsha: National University of Defense Technology, 2012: 51−64. (in Chinese)
[15] HE B Y. Analysis approaches for precision reachable sets of manned lunar orbits using numerical continuation theory. Changsha: National University of Defense Technology, 2018: 54−80. (in Chinese)
[16] LI J Y, GONG S P, BAOYIN H X. Generation of multi-segment lunar free-return trajectories. Journal of Guidance, Control, and Dynamics, 2013, 36(3): 765–775.
[17] HE B Y, LI H Y, ZHOU J P. Solution domain analysis of Earth-Moon quasi-symmetric free-return orbits. Transactions of the Japan Society for Aeronautical Space Sciences, 2017, 60(4): 195–201.
[18] LI Z J, GUO L L, PENG K. Research on site selection of manned lunar base. Manned Spacecraft, 2015, 21(2): 158–162. (in Chinese)
[19] IZZO D, MARTENS M, PAN B. A survey on artificial intelligence trends in spacecraft guidance dynamics and control. Astrodynamics, 2019, 3(4): 287–299.
[20] IZZO D, HENNES D, SIMOES L F, et al. Designing complex interplanetary trajectories for the global trajectory optimization competitions. Space Engineering, 2016, 114: 151−176.
[21] URIOT T, IZZO D, SIMOES L F, et al. Spacecraft collision avoidance challenge: design and results of a machine learning competition. Astrodynamics, 2022, 6(2): 121–140.
[22] LI H Y, CHEN S Y, IZZO D, et al. Deep networks as approximators of optimal low-thrust and multi-impulse cost in multitarget missions. Acta Astronautica, 2020, 166: 469–481.
[23] PENG H, BAI X L. Artificial neural network–based machine learning approach to improve orbit prediction accuracy. Journal of Spacecraft and Rockets, 2018, 55(5): 1248–1260.
[24] ZHU Y H, LUO Y Z, YAO W. Fast accessibility evaluation of the main-belt asteroids manned exploration mission based on a learning method. Proc. of the IEEE Congress on Evolutionary Computation, 2018. DOI: 10.1109/CEC.2018.8477849.
[25] ZHU Y H, LUO Y Z. Fast approximation of optimal perturbed long-duration impulsive transfers via artificial neural networks. IEEE Trans. on Aerospace and Electronic Systems, 2020, 57(2): 1123–1138.
[26] YANG F Y X, YANG L P, ZHU Y W, et al. A DNN based trajectory optimization method for intercepting non-cooperative maneuvering spacecraft. Journal of Systems Engineering and Electronics, 2022, 33(2): 438−446.
[27] CHENG L, LI H N, WANG Z K, et al. Fast solution continuation of time-optimal asteroid landing trajectories using deep neural networks. Acta Astronautica, 2020, 167: 63–72.
[28] LI X F, DONG L, SUN C Y. Hybrid Q-learning for data-based optimal control of non-linear switching system. Journal of Systems Engineering and Electronics, 2022, 33(5): 1186−1194.
[29] HORNIK K. Approximation capabilities of multilayer feedforward Networks. Neural Networks, 1991, 4(2): 251–257.
[30] BERRY R. Launch window and translunar, lunar orbit, and transearth trajectory planning and control for the Apollo 11 lunar landing mission. Proc. of the 8th Aerospace Sciences Meeting, 1970: 24.
[31] MENG Z F, GAO S, WANG Z S, et al. Circumlunar free return trajectories design and validation for high-speed Moon-to-Earth reentry mission. Science Sinica Technologica, 2015, 45: 249–256. (in Chinese)

Biographies

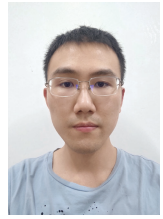

YANG Luyi was born in 1995. He received his bachelor degree in aerospace engineering from National University of Defense Technology, in 2017. Then he was enrolled in a combined "Master+PhD" program and he is a doctoral candidate in the College of Aerospace Science and Engineering, National University of Defense Technology since 2019. His research interests are trajectory design and optimization of the manned lunar mission, and combining deep learning with trajectory design method.
E-mail: yangluyi@nudt.edu.cn

LI Haiyang was born in 1972. He received his Ph.D. degree from the School of Aerospace Science and Engineering, National University of Defense Technology, in 2000. Currently he is a professor in National University of Defense Technology. His research interests include aircraft design, mission scheduling, and analysis of the manned spacecraft system.
E-mail: lihaiyang@nudt.edu.cn

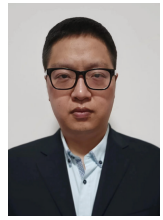

ZHANG Jin was born in 1983. He received his Ph.D. degree from the School of Aerospace Science and Engineering, National University of Defense Technology, in 2013. Currently he is an associate professor in National University of Defense Technology. His research interests include astrodynamics and space mission planning.
E-mail: zhangjin@nudt.edu.cn

ZHU Yuehe was born in 1990. He received his Ph.D. degree from the School of Aerospace Science and Engineering, National University of Defense Technology, in 2020. Currently he is a lecturer in National University of Defense Technology. His research interest is space mission planning for large-scale object visiting.
E-mail: zhuyuehe@nudt.edu.cn